SciTech2015
5-9 January, 2015, Kissimmee, FL
53rd AIAA Aerospace Sciences Meeting

Analysis of a Low Boom Supersonic Flying Wing Preliminary Design

Jiaye Gan*, Gecheng Zha†
Dept. of Mechanical and Aerospace Engineering
University of Miami
Coral Gables, FL 33124
gzha@miami.edu

Abstract

This paper presents the numerical analysis of a low boom supersonic bi-directional flying wing (SBiDir-FW) preliminary design to demonstrate the advantages of the concept. The mission requirements include cruise Mach number of 1.6, cruise altitude around 50kft, payload of 100 passengers, and a range of 4000nm. The gross takeoff weight is about 197kLb. The configuration is a flying wing symmetric about both the longitudinal and span axes. The sweep angle varies from 82° at the very leading edge to 78° at the tip. Two designs with same sweep angles and planform shapes are presented by varying airfoil meanline angle distributions to achieve different overpressure signatures and L/D ratios. The first design D82-78.4 achieves an L/D of 8.16, C_L of 0.54, and the ground sonic boom noise level of 71.7PLdB. The second design D82-78.8 increases the C_L and L/D with C_L =0.60 and L/D = 8.54, while keeping a low level of ground sonic boom at 71.9PLdB by cruising at a little higher altitude of 52kft. A typical near field overpressure signature has a strong shock wave followed by a strong expansion in the overall process of expansion. The strong shock-expansion is mostly canceled out by themselves during the process of the wave propagation to ground. The designs indicate that the overpressure signature and aerodynamic efficiency are very sensitive and controllable by the variation of meanline angle distributions of the airfoils. This is an important relationship between the geometry parameters and the sonic boom/aerodynamic efficiency so that a design optimization strategy can be developed. All the designs with varied meanline angle distributions in this paper are conducted manually. With the encouraging results achieved so far, it is believed that the NASA's N+2 and N+3 goal to have ground sonic boom below 70PLdB for a supersonic civil transport is close to reach if a systematic design optimization is conducted.

* Ph.D. Candidate
† Professor, AIAA Associate Fellow

1 Introduction

The major challengers of supersonic transports (SST) may be summarized as sonic boom, aerodynamic efficiency, and airport noise.

1.1 Aerodynamic Efficiency

One factor affecting supersonic aerodynamic efficiency is the wave drag. The other factor is the large flight speed disparity between take-off/landing and cruise. At take-off and landing, the low flight speed requires a high aspect ratio (AR) and low wing sweep angle. High-speed cruise however requires the opposite characteristics. A compromise is hence required and it hurts the supersonic cruise efficiency.

The oblique flying wing (scissor wing) is to overcome the speed disparity by rotating the wing up to 60° above a fuselage[1, 2]. However, scissor wing is asymmetric about the flight direction and could have serious stability and control problems[3, 4, 5, 6, 7]. The feasible maximum Mach number of scissor wing is limited to 1.3-1.4[8]. The other concept to tackle the speed disparity is the variable sweep wing or swing wing as used in F-14. A part of the wing will be rotated forward to reduce sweep angle and increase aspect ratio at low speed. However, it comes with a heavy penalty due to the increased weight of the mechanical and control system. In addition, a delta wing usually has a small wing area and there is not much area that can be used for swing wing. The aspect ratio increase is hence quite limited. Both the scissor wing and swing wing configurations are not adopted by Boeing and Lockheed Martin for their N+2 and N+3 designs[8, 9, 10, 11, 12].

1.2 Airport noise

The high airport community noise of a SST is primarily due to its higher engine jet speed than a subsonic airplane. One reason is that a SST does not use high bypass fan engines to avoid large capture area drag. The thrust hence is primarily generated by the high exhaust jet speed and momentum. The other reason is that a supersonic airplane wing usually has high sweep angle and low aspect ratio, which hurt the low speed performance with significantly reduced L/D, C_{Lmax}, and the slope of C_L vs AoA. It results in high stall speed, large required thrust to accelerate the airplane, and high engine jet speed that generates high airport noise. For example, Concorde's wing aspect ratio is 1.7, which is one important factor for the high airport noise.

1.3 Sonic boom

Sonic boom appears to be the most challenging problem to overcome for SST design. Sonic boom is the noise that propagates to ground as a N-wave created by the shock waves of a SST. Sonic boom is caused by volume blockage and lift. Airplane lift requires high pressure on the lower surface (pressure surface) and low pressure on the upper surface (suction surface). The high pressure will generate acoustic compression waves or shock waves and the low pressure will generate acoustic expansion waves. Since a compression wave always has a slightly higher wave speed and Mach cone angle than the compression wave immediately upstream, they have the tendency to merge in the mid-field or far-field to form a shock wave. If both the front and tail

compression waves or shock waves coalesce, they become stronger shock waves and appear on the ground as a N-wave.

In general, the longer and smoother the lift is distributed, the slower the overpressure will rise, and the less intense the compression waves will coalesce. The equivalent area theory of Jones-Seebass-George-Darden (JSGD)[13, 14, 15, 16, 17, 18] is intended to provide a guideline to control the lift and volume distribution to obtain desirable overpressure[12]. It is possible that the compression waves will not coalesce if the overpressure compression is smooth and gradual. In that case, a smooth *Sine* wave shape overpressure signature will be obtained on ground instead of a N-wave.

Currently, there are in general two strategies for boom mitigation. The first is based on the flat-top signature of JSGD theory to implement nose bluntness, which creates a shock distribution with the greatest strength near the aircraft and the shocks are weakened gradually due to interaction with expansion waves from the blunt nose as they travel to the ground. However, this design also induces substantial wave drag since the entropy increase due to the strong shock waves is irreversible. The Boeing's N+2 design appears to adopt the flat-top overpressure signature strategy[8, 9]. The second strategy is based on the ramp overpressure signature of JSGD theory to use a sharp nose in order to generate weak shocks. In principle, weak shocks are more likely to achieve low wave drag. Darden investigated nose-blunt relaxation as a compromise between the blunt nosed low-boom aircraft and sharp nosed low drag design[18]. The Quiet Spike^{TM} of Gulfstream[19] and Lockheed Martin's N+2 designs[20, 11] adopt the sharp nose strategy. The aforementioned swing wing and scissor wing are aimed at improving subsonic performance and reducing supersonic wave drag, and are not intended for boom mitigation.

However, the linear equivalent area theory also has a few limitations: 1) The overpressur signature always begins and ends with a shock wave as assumed by Whitham[21] for a supersonic projectile with body of revolution. Such overpressure signature tends to lead to a convex body of revolution such as a conventional fuselage. It may exclude the lifting surface configurations that are aligned with freestream and begin and end with acoustic compression waves instead of shock waves. 2) The complicated wave system propagation in atmosphere from the mid-field to ground is not linear. The "optimum" flat-top and ramp over-pressure signature may not be truly optimum for a realistic aircraft boom mitigation. 3) The linear equivalent area rule does not directly link to a realistic wing-tube configuration. Error in equivalent area matching has unpredictable effect on ground boom signature[22]. It is difficult to specify the required lift distribution with wing-body interference to use linear equivalent area rule. 4) The linear equivalent area theory does not consider drag. Following the optimum mid-field overpressure signature makes it difficult to minimize drag[22].

In 2008, NASA outlined the requirements of N+2 (year 2020-2025) and N+3 (year 2030-2035) goal of supersonic civil transport[23]. The N+2 mission goal includes: the range $\geq$ 4000nm, Mach number =1.6-2.0, passenger 25-100. For N+3, the range $\geq$ 4000nm, Mach number =1.3-2.0, passenger 100-200. The most challenging requirement for both N+2 and N+3 is the sonic boom noise level (based on linear theory) should be between 65 to 70 dBPL. NASA contracted Boeing [8, 9] and Lockheed Martin [24] to conduct design of N+2 supersonic airplane. Both the designs have good aerodynamic performance, but the sonic boom levels are at about 80-85dBPL[9, 10, 11], still quite distanced from the targeted 65 to 70 dBPL. Welge et al [8, 9] present Boeing's projected supersonic civil transports up to N+3 in 2040, which indicates that their configurations for the next 3 decades will be mostly the same tube-wing configuration with the difference in the details and refinement.

To satisfy the challenging requirements of future SST, a technology breakthrough that can significantly reduce sonic boom, airport noise, and increase fuel efficiency is needed. Current efforts indicate that even making a small business jet to satisfy the sonic boom requirements is arduous. It would be more difficult to apply the same technology to large supersonic airplane such as for 200-300 passengers.

Zha and his team recently have suggested a new concept of Supersonic Bi-Directional Flying Wing (SBiDir-FW)[25, 26, 27, 28, 29], which has a great potential to mitigate sonic boom and airport noise, improve aerodynamic efficiency, and substantially reduce aircraft weight. The basic concept of the SBiDir-FW is to maximize the length of lift distribution by a diamond shape flying wing to mitigate sonic boom and wave drag. Since SBiDir-FW is a new concept, little prior knowledge on the correlation between the geometry and sonic boom and aerodynamic performance is available. A trade study is conducted in [25] to develop such a correlation. The trade study includes the variation of sweep and dihedral angle, meanline angle distribution, leading and trailing edge thickness, and angle of attack. The trade study concludes that the sweep angle is very effective to increase lift coefficient and L/D. Generally speaking, within the Mach cone, the smaller the sweep angle, the higher the L/D. For example, a design with varying sweep angle from 84° to 68° and cruise Mach number of 1.6 achieves L/D of 10.4, but the sonic boom ground loudness is also high at 95PLdB[25] . When the sweep angle and airfoil thickness are fixed, the streamwise lift distribution is critical to determine the shock strength and far-field compression wave coalescing. An effective means to determine the streamwise lift distribution is to control the airfoil meanline angle distribution. The trade study in [25] shows that the SbiDir-FW configuration can achieve high aerodynamic efficiency without difficulties. Achieving low boom design appears to be much more challenging.

The purpose of this paper is to conduct more detailed analysis of a low boom SBiDir-FW configuration with the sweep angle and planform fixed to study the airfoil meanline angle distribution effect on sonic boom and aerodynamic efficiency. This flying wing has a payload of 100 passengers, a range of 4000nm, and at cruise altitude around 50kft.

2 The Supersonic Bi-Directional Flying Wing Concept

The airplane is a flying wing configuration with a symmetric planform about both the longitudinal and span axes with two flight directions altered by 90°. At subsonic flight, the planform will rotate 90° from the supersonic mode shown in Fig. 1 to the subsonic mode as shown in Fig. 2. Fig. 3 shows the 3D supersonic flight direction and the thin airfoil highlighted to form the flying wing to achieve low wave drag. Fig. 4 shows the subsonic mode after 90° rotation from the supersonic mode also with the subsonic airfoil highlighted. A reversed rotation will be done when the mode is changed from subsonic to supersonic. Since the span is significantly shorter than the length, the subsonic airfoil will be significantly thicker than the supersonic airfoil as shown in Fig. 4 to provide high lift coefficient needed for subsonic flight.

The engines will not be rotated and will be always aligned with the flight direction. The rotating turbomachinery inside the jet engines also provides the gyroscope effect to enhance the engine stability. The yaw moment to rotate the airframe will be generated by ailerons or split-flaps on the two sides of the flying wing. No powered driving system is needed to rotate the airframe and hence the weight penalty can be avoided. The engines can be located at or off the geometric center to shift the center of gravity during different mode of flight as needed.

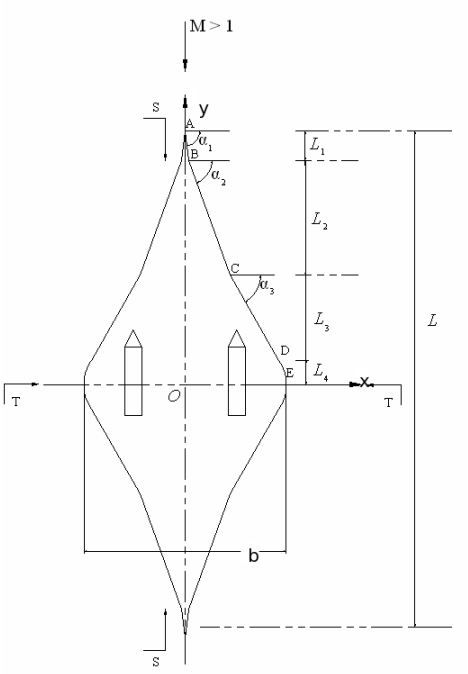

Figure 1: Sketch of a SBiDir-FW Planform flying in supersonic mode (not to scale)

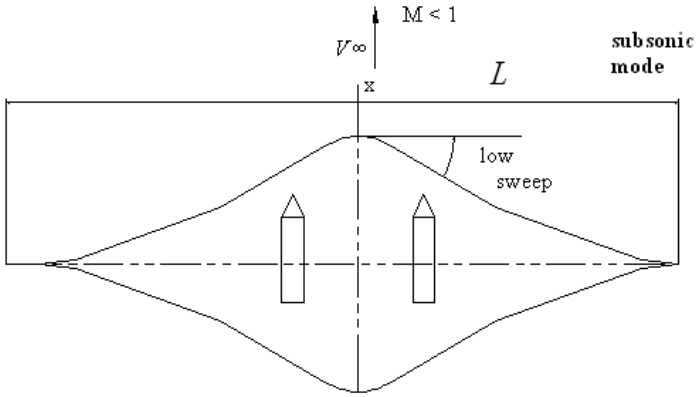

Figure 2: Sketch of a SBiDir-FW Planform flying in subsonic mode (not to scale)

The pitching and rolling moment will be also generated by ailerons and flaps to achieve tailless flight. The desirable transition mode Mach number is high subsonic such as about 0.8 to avoid the unsteady force introduced by shock waves at supersonic speed.

The feasibility of mode rotation transition is not a question any longer after the demonstration of the award winner "Rotating Dragon" drone in Beijing Air Show on Sept. 25, 2013. Rotating Dragon is designed and made by Chendu Aircraft Company in China and its planform is symmetric about both the longitudinal and span axis with a subsonic cruise Mach number. It can freely rotates 90° in the air. However, only supersonic flight will benefit significantly from the planform rotation. It is not clear if they intend to develop supersonic aircraft as the next step.

After the 90° rotation, the subsonic aspect ratio (AR) will be substantially increased by $(\frac{L}{b})^2$ based on the following relation:

$$AR_{M<1} = (\frac{L}{b})^2 \times AR_{M>1} \tag{1}$$

where L is the airplane length and b is the span in supersonic direction. Moreover, the sweep angle at subsonic will be largely reduced as the following:

$$\delta_{M<1} = 90^o - \delta_{M>1} \tag{2}$$

To make the flying wing symmetric about both axes, the airfoil stacked is also symmetric as highlighted in Fig. 3 and 4. The symmetric planform will let the trailing edge become leading edge during the rotation and generate lift to stabilize the mode transition. Even though a thin airfoil is used to stack the flying wing in the supersonic direction, sufficient volume can be easily

achieved due to the long length of the flying wing body, which is also the chord of the flying wing airfoil.

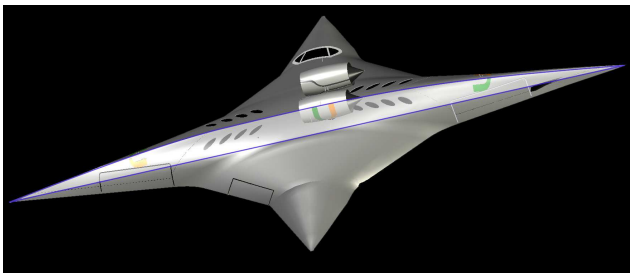

Figure 3: A SBiDir-FW civil transport in supersonic mode flying toward right, supersonic thin airfoil highlighted in the middle.

Figure 4: A SBiDir-FW civil transport in subsonic mode flying toward right, subsonic thick airfoil highlighted in the middle.

2.1 The Advantages

The SBiDir-FW has the following inherent aerodynamic and structural advantages over conventional wing-tube configurations. Because of them, the design philosophy could be very different from the conventional design.

2.1.1 Ultra Slenderness at Supersonic Mode

Comparing a diamond wing as sketched in Fig. 1 with a conventional delta wing with the same sweep angle and planform area, a diamond wing will have an aspect ratio half of that of the delta wing, a length $\sqrt{2}$ time longer and a wing span $\sqrt{2}/2$ time shorter. Comparing a SBiDir-FW with a conventional SST with the same length, the lift distribution length for SBiDir-FW is the whole airplane, whereas, a conventional SST's fuselage generates little lift and thus the lift distribution will be focused only on the wing portion. In fact, the supersonic zero span wing section of a SBiDir-FW, which has the longest chord and is equivalent to the "fuselage" of a conventional wing-tube configuration, generates the most lift and is crucial to determine the lift distribution for sonic boom.

The high slenderness and long lift distributing length are all beneficial to reduce shock strength, mitigate coalescing of compression waves in the mid-field, and ultimately minimize the sonic boom and wave drag. Thanks to supersonic aerodynamics characteristics that disturbance only propagates downstream, a small aspect ratio brings little induced drag penalty. The SBiDir-FW concept is particular suitable for the airplane carrying a large number of passengers such as 200-300. The longer the length, the thinner the airfoil thickness $(t/c)_{max}$ will be since the headroom for large or small airplane is about the same.

In addition, since the whole airframe is a lifting surface, it can be designed to have acoustic compression waves at the leading and trailing edge of the aircraft instead of shock waves of the conventional configurations. The advantages of acoustic compression waves are two folds: 1) Acoustic compression waves have slower wave speed than shock waves. It is thus more likely not

to coalesce in the mid-field than shock waves if the overpressure rise is not too high; 2) Acoustic compression waves are nearly isentropic and thus have smaller wave drag than shock waves.

2.1.2 High Aspect Ratio at Subsonic Mode

As indicated by Eq. (1) and (2), the smaller the supersonic aspect ratio, the higher the subsonic aspect ratio; the larger the supersonic sweep angle, the smaller the subsonic sweep angle. The conflict of subsonic and supersonic aerodynamic performance of conventional tube-wing configuration could be hence removed by rotating the airplane 90°. Designers can thus favor the supersonic aerodynamic performance as much as they like and do not have to compromise for subsonic performance. High supersonic aerodynamic performance could be naturally translated to high subsonic performance. Conventional supersonic wing-tube configurations usually do not use aspect ratio smaller than 1.5. Otherwise, it will be very difficult to takeoff and land at low speed. For SBiDir-FW, a typical supersonic aspect ratio is about 0.4, which translates to subsonic aspect ratio over 10-14, comparable to Boeing 787's aspect ratio of 11.2. It is also substantially greater than swing wing's maximum aspect ratio that is typically less than 6.5. At takeoff, the high subsonic aspect ratio could provide SBiDir-FW with higher L/D, higher maximum lift coefficient, lower stall velocity, lower required thrust, lower engine jet velocity, and hence lower airport noise than conventional SST. The upper surface mounted engines have the advantage that the jet noise is radiated mostly upward due to the shielding effect of the airframe body. With the high aspect ratio and upper mounted engines, the airport noise of a SBiDir-FW is expected to be significantly lower than a conventional wing-tube SST configuration.

2.1.3 Large Weight Reduction

Since a flying wing configuration uses the whole body area as lifting surface, it minimizes the volume, area and weight. Eq. (3) is an empirical wing weight formulation extracted from various different airplanes by Staton in late 1960s [30, 31, 32]. This weight estimation model is validated with the Concorde empty weight and good agreement is obtained.

$$W_{wing} = C_1 C_2 C_3 W_{dg}^{C_4} n^{C_5} S_w^{C_6} A^{C_7} (t/c)^{C_8} (C_9 + \lambda)^{C_{10}} (cos\Lambda)^{C_{11}} S_f^{C_{12}} q^{C_{13}} W_{fw}^{C_{14}} \tag{3}$$

To save space, only two of the parameters in Eq. (3) that distinguish a SBiDir-FW from a conventional supersonic airplane configuration are discussed herein. The first is A, the aspect ratio, with the coefficient $C_7 = 0.5$. The other is Λ, the sweep angle of the maximum thickness line, with the coefficient $C_{11} = -1$. For a conventional SST, a typical value of A is about 2 and Λ is about 60°. For a SBiDir-FW, a typical value of A is about 0.4 and Λ is always 0°. If assuming all other parameters are the same, the weight of a conventional SST wing will be 2.23 times greater than that of a SBiDir-FW due to the aspect ratio difference, and 2 times greater due to the maximum thickness line sweep angle. All together, the conventional wing weight will be 4.46 times greater if the wing planform areas are the same. Assuming opening passengers doors will increase weight by 20%, and pressurizing the cabin will increase weight by another 20%. The weight reduction of SBiDir-FW is still at the order of 68%. Eq. (3) is empirical and the quantitative results may be not precise, but the dictated relationship among the parameters is believed to be correct. Furthermore, a SBiDir-FW configuration removes the fuselage, which is another very significant weight reduction. The reduced weight will decrease fuel consumption and benefit sonic boom mitigation since the lift will be lower.

2.1.4 Applicable to Hypersonic Vehicles

The same principle and advantages of SBiDir-FW also apply to hypersonic flight such as one-stage to orbit reusable vehicles to have low wave drag at hypersonic and high lift and controllability at take off/landing at regular airports.

3 Mission Requirement

To implement realistic constraints for this conceptual design using SBiDir-FW, the mission requirement include cruise Mach number of 1.6, pay load of 100 passenger with standard luggage, and range of 4000nm. The text book *Design of Aircraft* by Corke [32] provides an excellent aircraft conceptual design methodology, which is adopted for the SBiDir design. A FORTRAN code was written based on this methodology in order to facilitate the design iterations.

To maximize the benefit of SBiDir-FW concept, a length of 100m is selected so that we can use thin airfoil with the thickness less than 3%, which will give sufficient headroom space and volume to hold passengers and fuel. It turns out that the volume is in general easy to achieve due to the inherent advantage of flying wing. Once the sweep and dihedral angles distributions are specified, the planform area is determined. When the complete SBIDir-FW geometry is determined and CFD analysis is completed, the coefficients of lift, drag, moment and the ratio of lift to drag are available. With all these geometry and aerodynamic performance parameters including engine fuel consumption, structure factor, and flight altitude as the input to the mission analysis code, an estimate of the aircraft weight at different flight stages is iterated by using standard estimates of the weight of passengers and crew, luggage, cockpit, engines, and other components. The range is one of the output results from the mission analysis.

In this design, the SBiDir configuration is expected to provide a very low wing loading, and thus short take-off and landing distances are expected. To choose the propulsion system, a computation of the overall aircraft drag is performed to ensure that the plane has sufficient thrust, and then engines that meet the thrust requirements are sized based on a reference engine.

4 Geometry Model

A geometry model is crucial to provide the required controllability to achieve loading distribution to minimize shock strength. In this research, an advanced geometry model is developed following the strategy for transonic and supersonic aircraft engine compressor/fan blades[33].

The wing is created by stacking a series of airfoil in spanwise direction along leading edge. A leading edge sweep and dihedral angle distribution can be specified at any leading edge point to determine the flying wing planform and aspect ratio. The airfoil is symmetric about the 50% chord location where the maximum thickness is located. Once the planform is determined, the most important step is to generate the meanline angle distribution of each airfoil, which will determine the actual meanline curves using a spline technique. Then the airfoil is formed by adding the thickness circles along the airfoil meanlines. The geometry model allows designers to freely adjust the meanline angel distribution to control the incidence angle, flow turning, loading distribution along the chord, and local expansion and shock waves. The airfoil thickness distribution from the leading edge to the maximum thickness is determined by a quarter-sine

wave distribution. The leading and trailing edge thickness are also required design parameters.

The meanline angle distribution adjustment and iteration is based on the airfoil surface isentropic Mach number distributions predicted by CFD, which shows the flow incidence, shock location, and shock strength. The design principle is to give the airfoil a small incidence to generate acoustic compression at the LE and a favorable flow turning distribution on the airfoil mid-chord that minimizes the peak Mach number and shock strength. A graphical user interface (GUI) is developed using Java to allow designers directly adjust the meanline angle distributions point by point using mouse click. All the designs are done manually so far to understand the physics and the relationship of sonic boom and aerodynamic efficiency with the design parameters.

5 Numerical Approach

The in house high order accuracy CFD code FASIP, which is intensively validated with various 2D and 3D steady and unsteady flows including sonic boom cases of bodies of revolution(NASA, Lockheed Martin) and NASA's delta wing configuration provided by the 2014 AIAA Sonic Boom Work Shop [25, 34, 26, 35, 36, 37, 38, 39], is utilized for the CFD analysis. To accurately capture shock waves and sonic boom, high order shock capturing schemes, including 3rd order MUSCL scheme[40], 3rd, 5th and 7th order WENO schemes and a finite compact scheme combining a shock detector and 6th order Padé scheme, are utilized in the code[37, 38, 39, 41]. A set of 4th order and 6th order central differencing schemes are devised to match the same stencil width of the WENO schemes for the viscous terms[42, 43]. The Roe's scheme [44] and a low diffusion E-CUSP scheme developed by Zha et al[45] are used as the approximate Riemann solver with all the different shock capturing schemes. For turbulent simulations, FASIP has implemented Detached Eddy Simulation (DES)[46, 47, 48, 49, 50, 51, 52], Large Eddy Simulation(LES)[43, 53], and Reynolds averaged Navier-Stokes (RANS)[54, 42, 55, 56, 57, 58, 59, 60]. An implicit 2nd order time accurate scheme with pseudo time and unfactored Gauss-Seidel line relaxation is employed for time marching. The MPI parallel computing is utilized and a high scalability is achieved[61].

The Euler inviscid solver, which is validated with accurate prediction of sonic boom, is used for design iterations at supersonic mode. The Euler solver also predicts lift and pressure drag accurately. The only drag missing from an Euler solver is the supersonic surface friction drag. Winter and Smith [62] conducted rigorous experimental study of supersonic friction drag for delta wings, which has the airfoil maximum thickness of 8.3%, Mach number from 1.5 to 2.6 and angle of attack (AoA0 up to 10°. The delta wing is tappered and twisted. His conclusion is that despite the wide variations in skin friction on the wing surface, the total skin-friction drag is probably only some 5 to 10 per cent less than that on a flat plate due to the adverse pressure gradient. The drag shows little variation with incidence.

Since the SBiDir-FW configurations simulated in this initial research do not include the propulsion systems, and the ranges of Mach number, sweep angle, AoA and airfoil thickness are all within the same range of Winter- Smith experiment[62], we hence adopt the flat plate surface friction coefficient modified for different altitude as the surface friction coefficient of SBiDir, which is on the conservative side of the drag estimate. The utilization of flat plate surface friction coefficient for SBiDir-FW design iteration not only saves tremendous CPU time of CFD simulation, it is also more reliable than the friction prediction from Reynolds averaged Navier-Stokes (RANS) solvers[63], which often have difficulty in accurately predicting drag. The same

way using flat plate friction coefficient for supersonic wing is also adopted by Seebass[64].

The viscous Navier-Stokes solver is used to predict the lift, drag (with both pressure and friction drag) and moments for the subsonic mode of SBiDir-FW, which has thick airfoil and flow separation. A flat plate friction coefficient would not be as accurate as for supersonic mode with thickness less than 3% and no flow separation.

The far field sonic boom propagation to ground is simulated using the the NASA *sBOOM* code, which has been intensively validated for sonic boom propagation[65].

6 Results

6.1 Low Boom Design

6.1.1 Overall Performance and configuration

The Design D82-78.4 achieves an excellent aerodynamic performance of L/D = 8.16 and a very low sonic boom of 71.7 PLdB at cruise altitude of 50000ft as shown in Table 1. Fig. 5 is the surface Mach number contours of the flying wing showing the overall configuration in supersonic flight mode.

Table 1: D82-78.4 performance

Range	Pass	Mach	Alt(ft)	W_{TO}(Lb)	EW(Lb)
4000nm	100	1.6	50000	196,543	95,833
Length(m)	Span(m)	Area(m^2)	Volume(m^3)	AR($M<1$)	AR($M>1$)
100	16.5	764	650	13.074	0.356
C_L	C_D	C_L/C_D	C_M		
0.05410	0.00663	8.15988	-0.00102		

Altitude(ft)	48000	50000	52000	56000	60000
Ground Boom PLdB	72.58	71.71	70.93	67.75	66.17

A variable sweep from 82° to 78° as indicated in Fig. 6 is utilized to have a supersonic aspect ratio of 0.356, which translates to a subsonic aspect ratio of 13.1. The cruise angle of attack(AoA) is 3°. The thickness of the 0% span airfoil is 2.2% and the airfoil thickness is decreased toward outerspan(see Fig. 6). With the length of 100m, it gives 2.2m height in most of the passenger cabin area. Fig. 7 shows the supersonic airfoils(left) from zero span to 90% span. It can be seen that all the airfoils are symmetric about the 50% chord point that is the span axis. On the right of Fig. 7 is the subsonic airfoils, which again are symmetric about the 50% chord point that is the longitudinal axis. Fig. 8 is the cabin assembly for 100 passengers including lavatories and crew cabin in the middle. The pink area is the seating area with minimum height of 1.8m. The configuration provides a total volume of $650m^3$. The volume excluding the cabin is far greater than needed for fuel storage. The gross weight is 196,543Lb with an empty weight of 95,833Lb.

6.1.2 Mesh

The mesh for the CFD Euler calculation is constructed using the H-mesh topology in order to achieve high quality around the sharp LE and TE of the airfoils. Half of the spanwise configura-

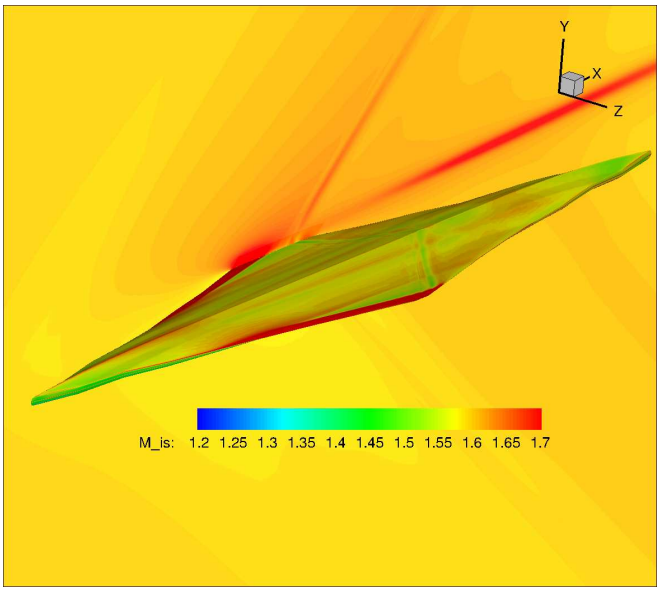

Figure 5: Surface Mach number contours of the Design D82-78.4 flying wing in supersonic mode.

tion is calculated due to the symmetric geometry. The mesh is inclined at the Mach cone angle and is refined on the body of the airplane as shown in Fig. 9. The far field boundary is located at $2.5C \times 5.5C \times 3C$ as indicated in Fig. 9, where C stands for the flying wing body length. Fig. 10 displays the zoomed mesh around the airplane body showing the local refinement to resolve the shock waves at the leading edge, trailing edge and on airfoil surface at about 2/3 chord location, where an oblique shock wave will emanate. The mesh does not only has the local refinement in the streamwise direction, it is also refined on the wing surface in the spanwise direction as shown on the right of Fig.10 to resolve a shock wave emanating from the wing tip. The mesh uses a total of 385 points in the streamwise direction, 129 in the spanwise direction, and 197 points in the direction normal to the wing surface. Total mesh size is 9.7 million points. Mesh refinement study indicates that the solution is converged based on mesh size.

6.1.3 Flow Field and Sonic Boom

The trade study in [25] indicates that meanline angle distribution is very important to control the loading distribution along the streamwise direction, which significantly affects the shock strength and sonic boom. The basic low boom design strategy is to weaken the surface shock waves in order to provide a favorable near field over-pressure signature, which will further reduce the ground sonic boom level. The meanline angle variation from LE to TE represents how much the flow is turned by the airfoil, which determines the streamwise lift and loading distribution of the airfoil.

Fig. 11 shows the meanline angle distributions at different span. At the inner span from 0 to 25%, the meanline angle is non-monotonic. The airfoils have a rapid turning in the first 20% of the airfoil, then experience a reversed cambering from 20% to 80% chord to minimize the peak Mach number and shock strength, and have the same turning as the first 20% chord at the last 20% chord.

The meanline angle is symmetric about 50% chord to satisfy the symmetry requirement of

SbiDir-FW planform. At the span outside 25%, the reversed cambering in the middle of the airfoil is reduced to about zero turning. The overall turning, i.e., loading, is reduced toward the outer span to the tip.

The 0% span airfoil has the role of the fuselage of a conventional airplane to hold the passengers. However, a large difference form the conventional supersonic airplane is that the zero span sustains most of the total lift of the flying wing since it is the longest and thickest airfoil, whereas a conventional fuselage generates little lift. The inner span has the longest chord length and is critical to determine the compression wave coalescing in the mid-field.

As displayed in Fig. 7, the supersonic airfoils at different span locations of the flying wing reflect the non-monotonic meanline meanline angle distributions. The airfoils have the general features with the leading edge up to 20% chord drooped down to accommodate the upward flow angle due to front compression wave with favorable incidence. The airfoils have large cambering and therefore large loading in the first 20% of the chord. The middle of the airfoils have either reversed cambering or little cambering as shown in Fig. 11 to reduce the peak Mach number and shock strength. Due to the symmetry requirement, the airfoils also have high loading at the last 20% of the chord.

Fig. 12 and 13 are the surface isentropic Mach number distribution at different span location. The 0% span airfoil has near zero incidence. The incidence is defined as the angle between the flow direction and the leading edge meanline tangential direction. Fig. 12 shows that the loading distribution is fairly uniform from the leading edge to the trailing edge at zero span. Such a loading distribution is favorable to mitigate the coalesce of compression wave that forms the shock wave in the far field. The incidence is increased toward the outer span due to the up wash of the flow.

Fig. 14 is the overpressure signature two body below of the flying wing calculated by the CFD. The front compression wave is smooth attributed to the even loading distribution shown in Fig. 12. The front compression is followed by a "flat-top" over pressure, which is obtained by the light loading in the middle of the airfoil. Followed the flat-top is a sharp expansion, which is interrupted by a strong shock wave near the end of the expansion. Immediately following the shock is another strong expansion, and then a weaker shock, and a weaker expansion. The pressure finally goes through a near "flat-bottom" and a gradual compression returning back to the ambient pressure.

Such a near field signature produces the ground overpressure signature shown in Fig. 15 calculated by the NASA sBOOM code[65]. Fig. 15 plots several altitudes from 46kft to 60kft. The ground signatures are fairly smooth and remain the flat-top wave shapes of the near field except with a small sharp tail at the beginning of the rear overpressure plateau. The ground overpressure signature are definitely not N-waves. The strong shock-expansion waves in the near field are canceled out when the overpressure signature propagates to the ground. As a result, the ground overpressure signatures do look like the desired flat-top wave shapes of JSGD theory, whereas the near field overpressure does not look like that due to the nonlinearity.

As shown in Table 1, the ground boom loudness begins with a low value of 72.6PLdB at cruise altitude of 48kft and is decayed to 66PLdB at the altitude of 60kft. The design cruise altitude is 50kft, which generates the sonic boom noise level of 71.7PLdB. If the range is reduced so that the same airplane can fly at 60kft, a really quiet sonic boom of 66PLdB is achieved.

Fig. 16 and 17 are the Mach contours at different span location showing the wave structures. Similar to the conclusion from Fig. 12, 13 and 14, the front shock is degraded to an isentropic

compression wave due to the very high sweep angle at leading edge and low incidence. This phenomenon is verified by CFD mesh refinement. After the initial compression wave, the flow experiences expansion on the suction surface and compression on the pressure surface. The expansion on suction surface is interrupted by an oblique shock to restore the pressure to ambient value. This is a typical shock wave structures for SBiDir-FW configuration. In other words, the strong shock is in the middle of the airplane instead of at the leading edge and trailing edge. The shock propagates circumferentially to pressure surface.

Fig. 18 is the Mach number contours on the suction surface and pressure surface. On the suction surface, the shock initiates from the wing tip and propagates toward the center span with decreasing shock strength.

On the pressure surface, there are strong expansion waves followed by a shock wave as reflected in the near field over pressure signature in Fig. 14. The contours indicates that flow does experience a strong shock, immediately followed by a strong expansion wave, and another weaker shock and weaker expansion as shown in the near field overpressure in Fig. 14. These shock-expansion tend to be canceled by themselves when propagating to ground as shown in Fig. 15.

6.2 Increased L/D

This section presents the second design, D82-78.8, which is intended to increase the L/D by modifying the meanline angle distribution while keeping the sweep angle and planform shape of D82-78.4 unchanged. Fig. 19 shows the meanline angle distributions of D82-78.8 at different span. Except the zero span, all the airfoil leading edge meanline angles are increased to enhance the overall loading (lift). Furthermore, the front and rear chord are more loaded by moving the turning points from 25%chord to 15%chord with a sharp turning instead of smooth turning. A slight reversed cambering is also introduced for most of the outer span sections to mitigate the peak Mach number and shock strength. Fig. 20 shows the supersonic airfoil shapes at different span for D82-78.8. Except the zero span, the airfoil toward the outer span has more bending, thus more lift loading, near leading and trailing edge than the D82-78.4. The middle part of the airfoils are lightly loaded to mitigate the shock strength.

Table 2 gives the overall performance of D82-78.8. The lift coefficient is increased from 0.054 to 0.06, an 11% improvement. The L/D is increased from 8.16 to 8.54, an 4.6% improvement. It is a significant aerodynamic performance improvement. The decreased weight due to higher L/D and increased lift makes the airplane able to fly at a higher altitude of 52kft. Table 2 indicates that at a low cruise alittude of 48kft, the ground sonic boom is higher than that of D82-78.4. However, at the designed altitude of 52kft, the boom loudness is significantly dissipated to 72PLdB, which is at a similar level of D82-78.4 at altitude of 50kft.

Table 2: D82-78.8 performance

Length(m)	Span(m)	Area(m^2)	Volume(m^3)	AR(subsonic)	AR(supersonic)
100	16.5	764	650	13.074	0.356
Cl	Cd	Cl/Cd	Cm		
0.06021	0.00705	8.54043	-0.00171		
Altitude(ft)	48000	50000	52000	56000	60000
Noise(PLdB,100m)	76.24	74.57	71.91	71.60	70.78

Fig. 21 is the chordwise isntropic Mach number distribution at different span locations. Since most of the leading edge menaline angle are higher than those of D82-78.4 except at zero span, the incidences are smaller for most of the span locations. Fig. 22 is the comparison of overpressure at the 2-body length below the airplane. The D82-78.8 has a slightly faster pressure rise in the front than D82-78.4. The flat-top is not maintained. The strong shock/expansion in the middle of the expansion wave still exists. The rear pressur plateau in general has a reversed shape of the front pressure plateau due to the symmetry of the geometry.

Fig. 23 is the ground overpressure signature propagated from different altitude. It shows that no N-waves are formed and the peak overpressure is dissipated with higher altitude. Fig. 24 compares the boom loudness of D82-78.4 and D82-78.8. From altitude 48kft to 60kft, the ground boom loudness decays by about 6PLdB for both the designs. The D82-78.4 has its boom noise dissipating faster at high altitude and D82-78.8 dissipates faster at lower altitude. This makes D82-78.8 cruising at 52kft have about the same boom level as D82-78.8 cruising at 50kft with about 72PLdB.

Fig. 25 and 26 are the Mach contours at different span location for D82-78.8. Again, there is no leading edge shock as the case of D82-78.4. Compared with the Mach contours of D82-78.4 in Fig. 16 and 17, two clear differences can be seen: The first is that the compression (green color) of D82-78.8 on the pressure surface starts after the front bending of the airfoil, whereas the D82-78.4 starts the compression immediately at the leading edge and the compression is longer and more uniform. D82-78.4 hence results in the flat-top near field overpressure signature. The second difference is that the expansion (red color) of D82-78.8 on the upper surface is significantly stronger with larger area. It indicates that D82-78.4 has higher overall speed on suction and hence greater lift. These differences are consistent with the meanline angle distributions that the D82-78.8 has smaller incidence and hence less compression at the very leading edge. However, since the overall meanline turning angles are greater, it has more expansion on suction surface.

Fig. 27 is the Mach number contours on the suction surface and pressure surface. On the suction surface, the shock initiates from the wing tip and propagates toward the center span with decreasing shock strength. Similar to the case of D82-78.4, the shock is immediately followed by expansion waves. Teh same wave system is propagated to the pressure surface.

7 Conclusions

This paper demonstrates that a supersonic bi-directional flying wing (SBiDir-FW) can achieve low sonic boom and excellent aerodynamic efficiency. Two designs with the same sweep angle and planform but different menaline angle distributions are presented. The mission requirements include cruise Mach number of 1.6, cruise altitude of around 50kft, payload of 100 passengers, and a range of 4000nm. The gross takeoff weight is about 197kLb. The configuration is a flying wing symmetric about both the longitudinal and span axes. The ultra-slenderness of the SBiDir-FW with the whole body being a wing significantly benefits the design to achieve smooth streamwise lift distribution in order to mitigate sonic boom. The empty structure weight is significantly reduced compared with conventional wing-tube configurations due to the very low supersonic aspect ratio and zero sweep angle of the maximum thickness line. The sweep angle varies from 82° at the very leading edge to 78° at the tip. The designs are intended to only change airfoil meanline angle distribution to achieve different overpressure signature and L/D.

Based on validated numerical simulation, the first design D82-78.4 achieves an L/D of 8.16,

C_L of 0.54, and the ground sonic boom noise level of 71.7PLdB. The second design D82-78.8 increases the overall turning by increasaing leading edge meanline angles for the outer span. The C_L and L/D are increased to C_L =0.60 and L/D = 8.54, while still keeping a low level of ground sonic boom at 71.9PLdB by cruising at a higher altitude of 52kft. The D82-78.4 has a flat-top near field overpressure signature due to the lower incidence and the compression starting right at the leading edge. The overall ground boom of D82-78.4 is lower than that of the D82-78.8. The gound boom loudness of D82-78.4 begins with 72.5PLdB at cruise altitude of 48kft and is decayed to 66PLdB at cruise altitude of 60kft. The D82-78.8 has higher gound boom loudness at 48kft, but the boom decays faster at low altitude and makes it suitable to fly at 52kft.

A typical near field overpressure signature has a strong shock wave followed by a strong expansion in the overall process of expansion. The strong shock-expansion is mostly canceled out during the process of the wave propagation to ground. The designs indicate that the overpressure signature and aerodynamic efficiency are sensitive to the varistion of meanline angle distributions of the airfoils. This is an important relationship between the geometry parameters and sonic boom/aerodynamic efficiency so that a design optimization strategy can be developed.

The SBiDir-FW configurations can achieve very high L/D (e.g. ≥ 10) fairly straightfordwardly by slightly decreasing the sweep angle. But the boom is also increased significantly. This paper does not present any effort on the very high L/D design. All the designs with varied meanline angle distributions are conducted by hand in this paper. It helps greatly to understand the physics, but is also very limited to find the optimum that needs to vary a large number of design parameters. With the encouraging results achieved so far, it is believed that the NASA's N+2 and N+3 goal to have ground sonic boom below 70PLdB for a supersonic civil transport is not far from reach if a sysmatic design optimization is conducted.

8 Acknowledgment

The funding support for this research from NASA NIAC grant NNX12AR05G8 is acknowledged. All the CFD simulation and design work are done at the Center for Computational Sciences(CCS) at University of Miami.

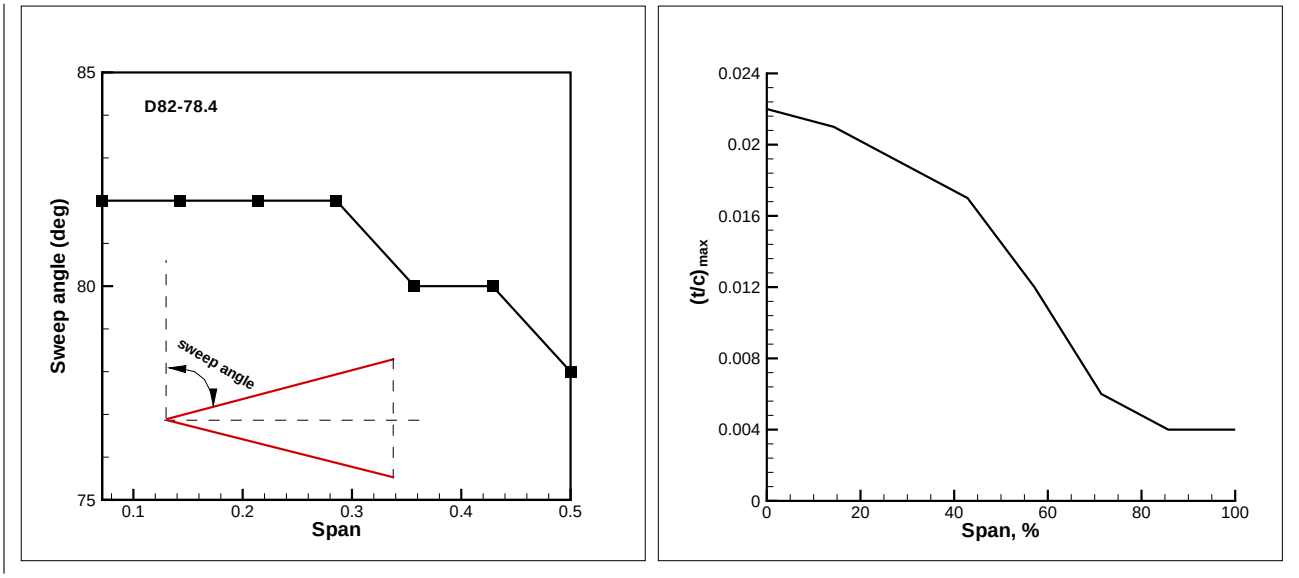

Figure 6: D82-78.4 spanwise distribution of leading edge sweep angle(left) and maximum thickness (right).

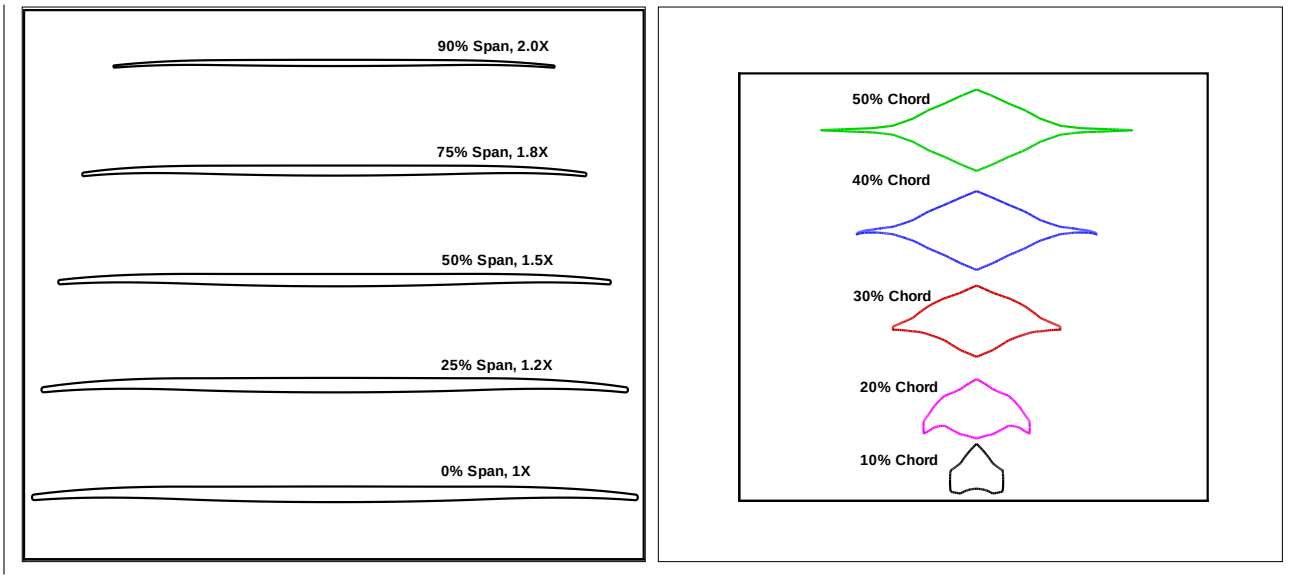

Figure 7: D82-78.4 symmetric supersonic airfoil shape(left) and subsonic airfoil shape(right).

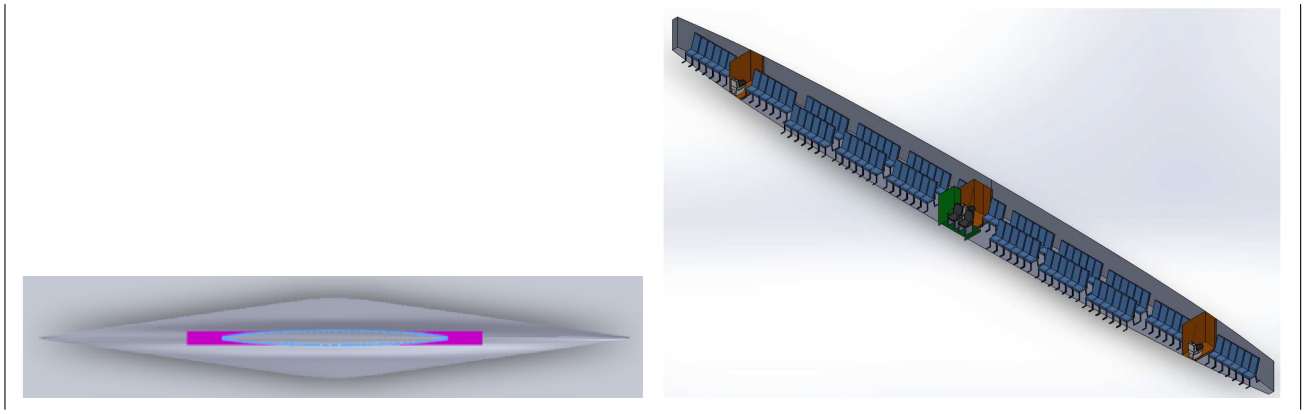

Figure 8: D82-78.4 cabin assembly for 100 passengers including lavatories and crew cabin in the middle.

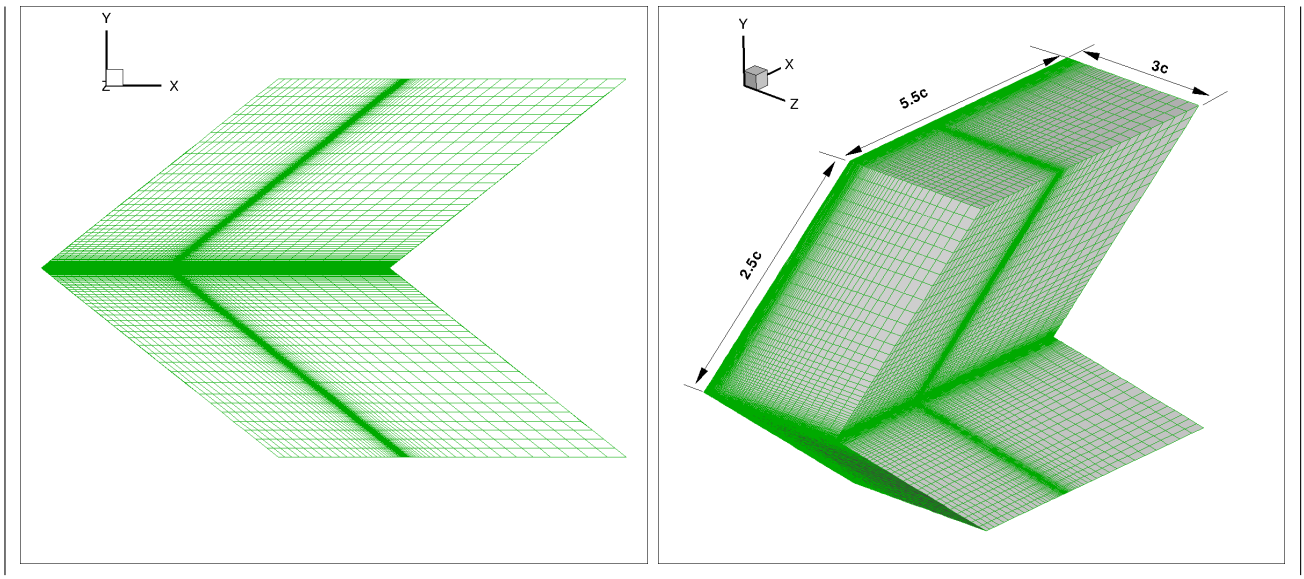

Figure 9: The mesh from side view (left) and the mesh at far field boundaries (right).

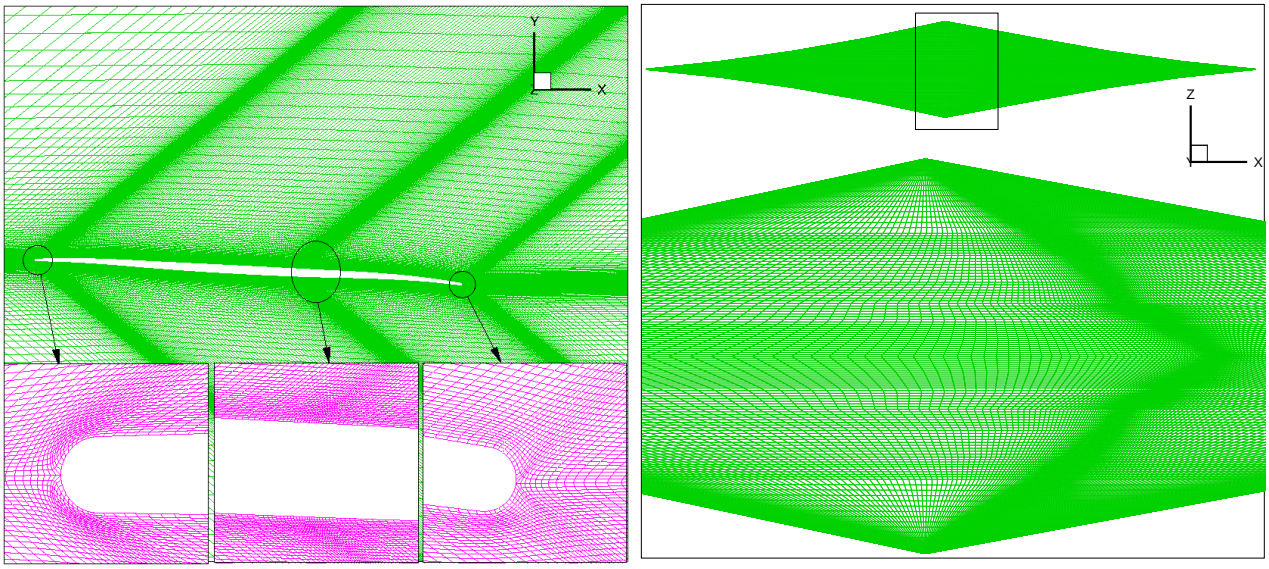

Figure 10: SBiDir mesh topology, streamwise plane (left), suction surface (right), Mesh size: $385 \times 129 \times 197 = 9.7M$.

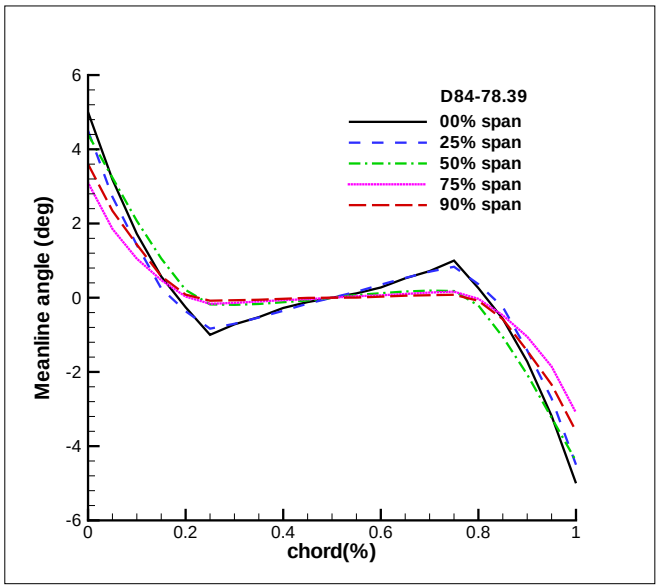

Figure 11: Meanline angle distribution of D82-78.4.

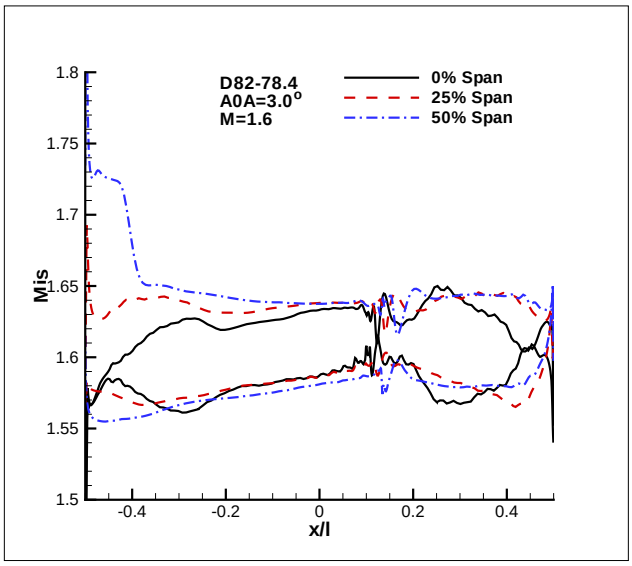

Figure 12: Surface isentropic Mach number distributions from 0 span to 50% span.

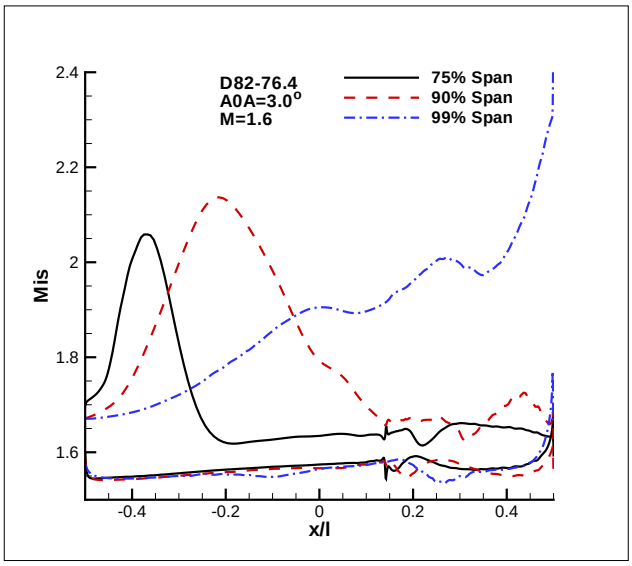

Figure 13: Surface isentropic Mach number distributions from 75% to 99% span.

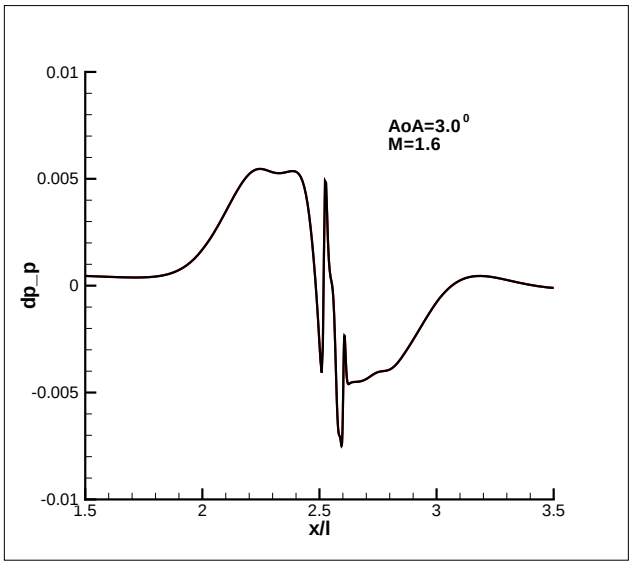

Figure 14: Overpressure two body length below, $\phi = 0°$.

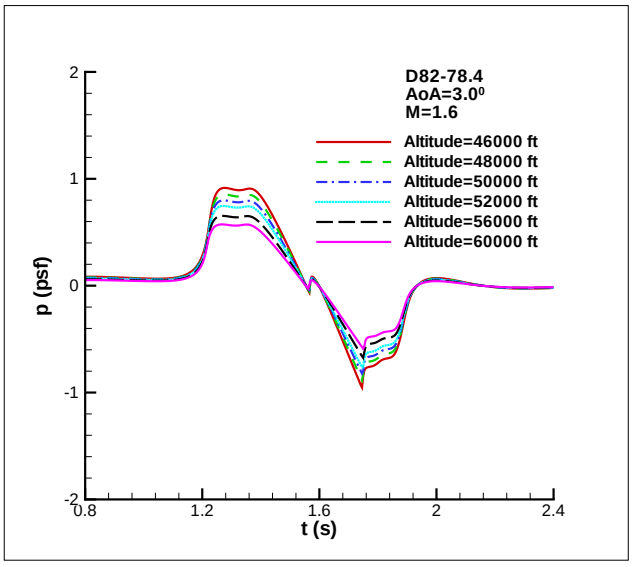

Figure 15: Ground overpressure sonic boom signature.

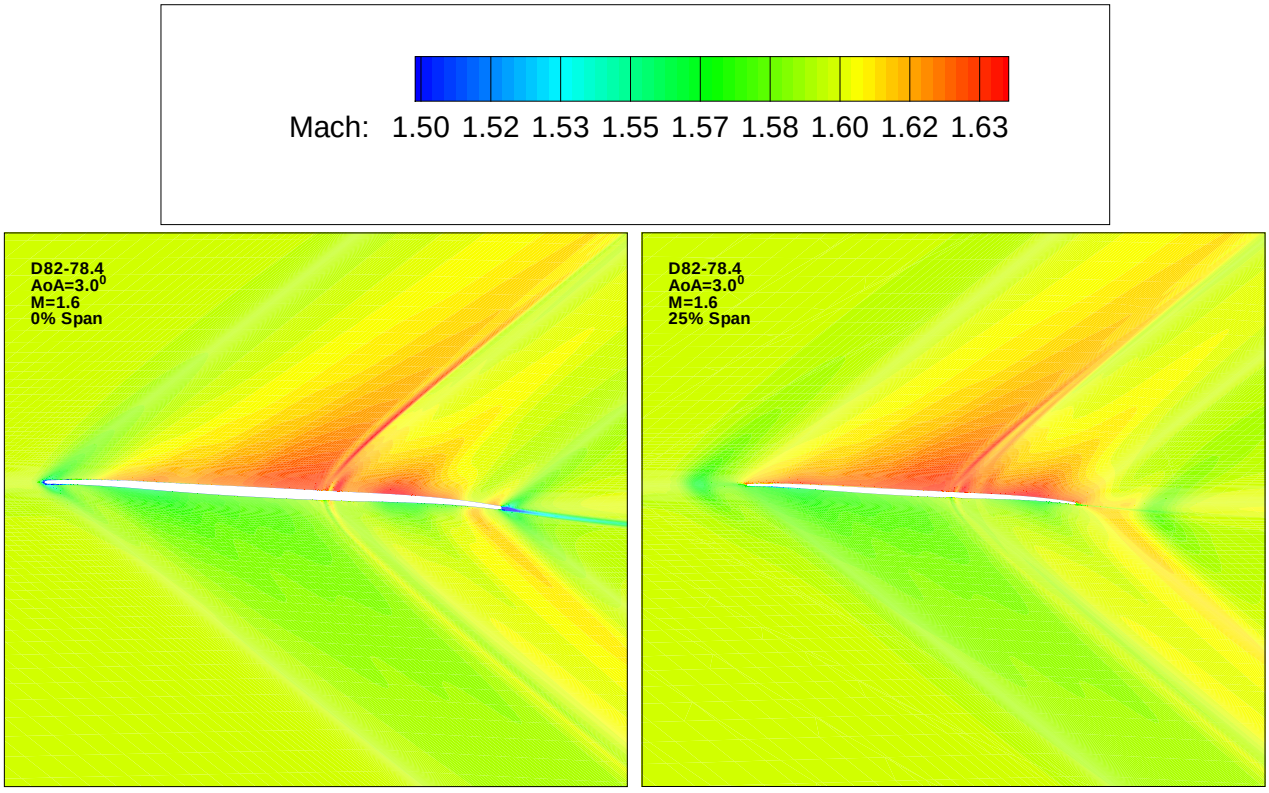

Figure 16: Mach number contours at 0 and 25% span.

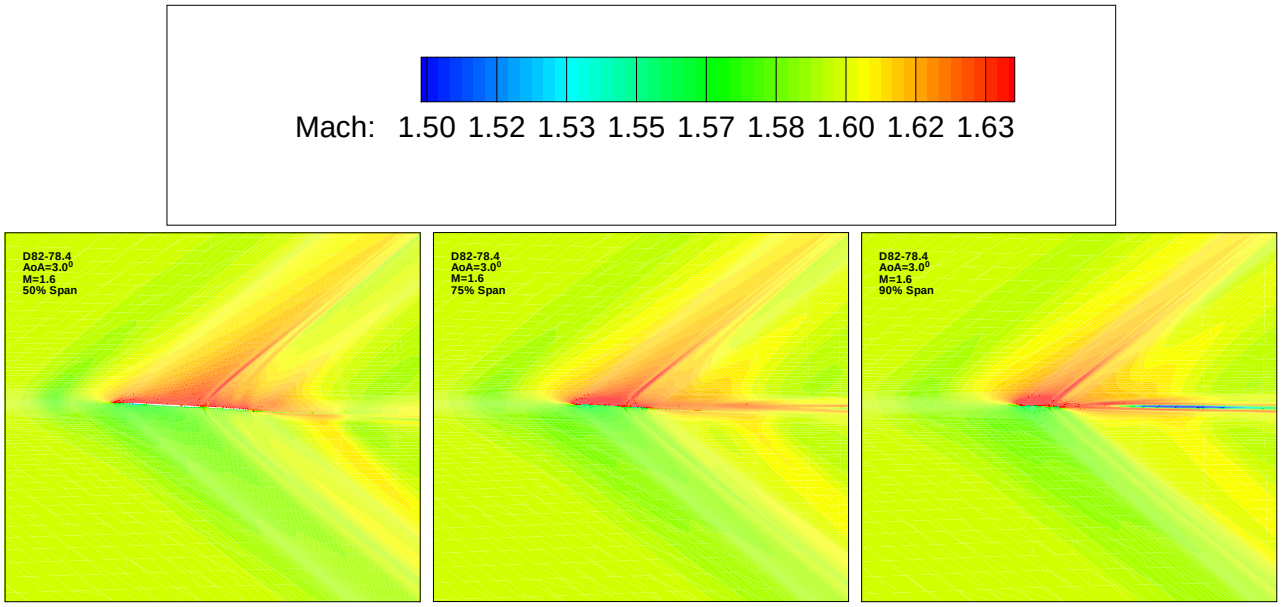

Figure 17: Mach number contours at 50%, 75% and 90% span.

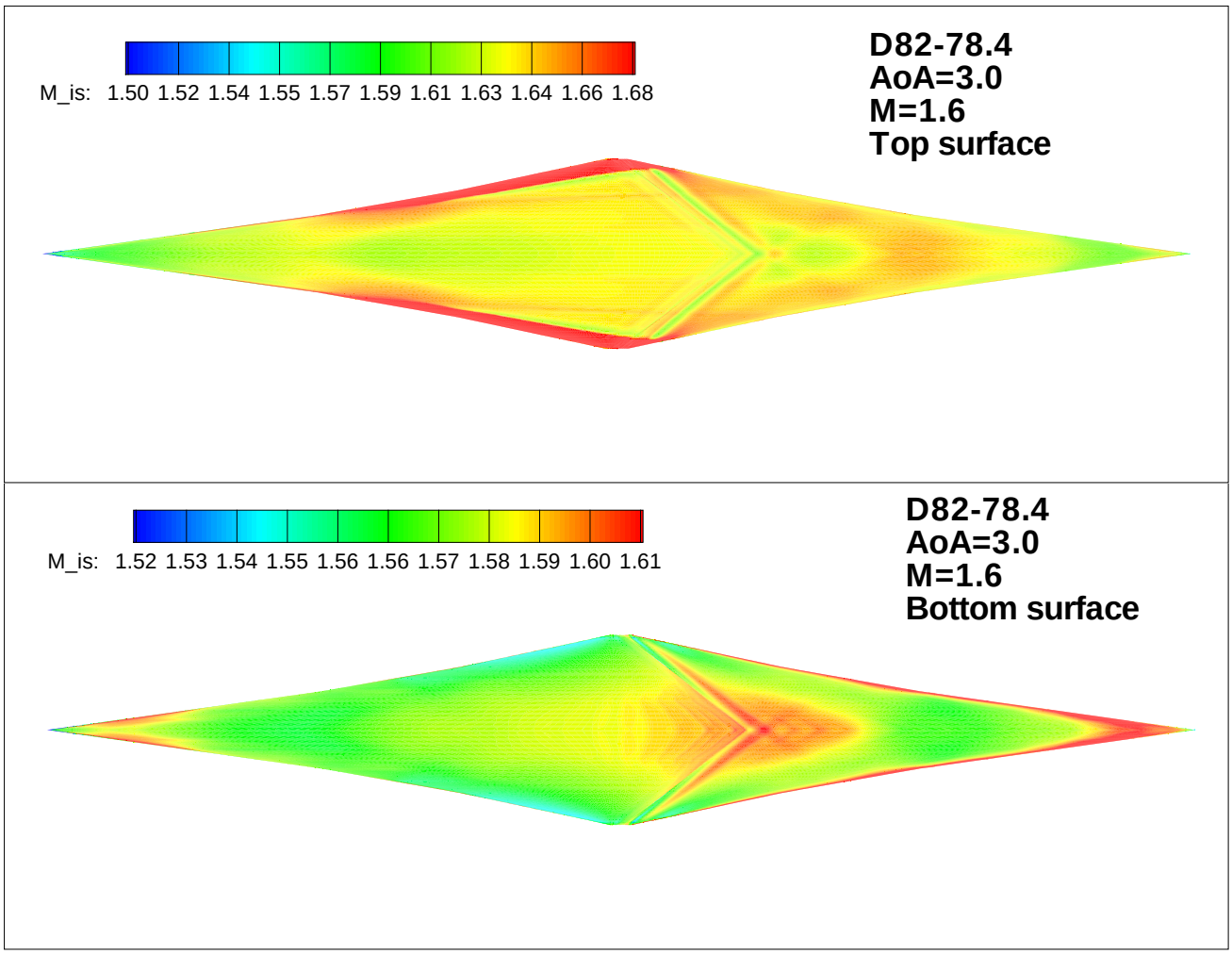

Figure 18: Suction (upper) and pressure (lower) surface isentropic Mach number contours.

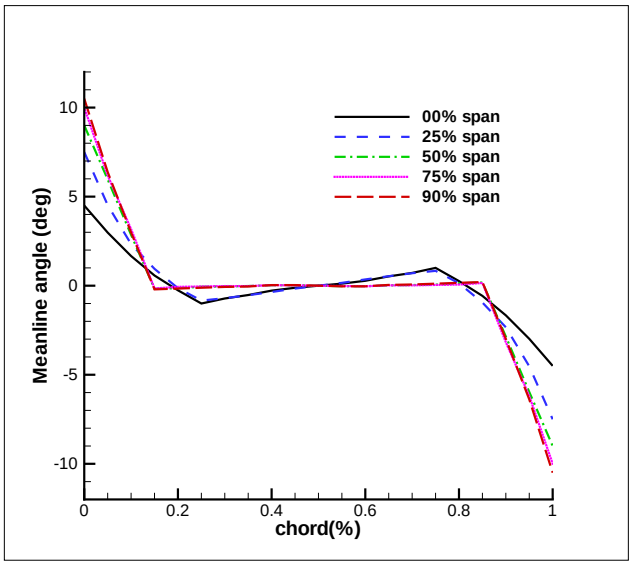

Figure 19: Meanline angle distribution of D82-78.8.

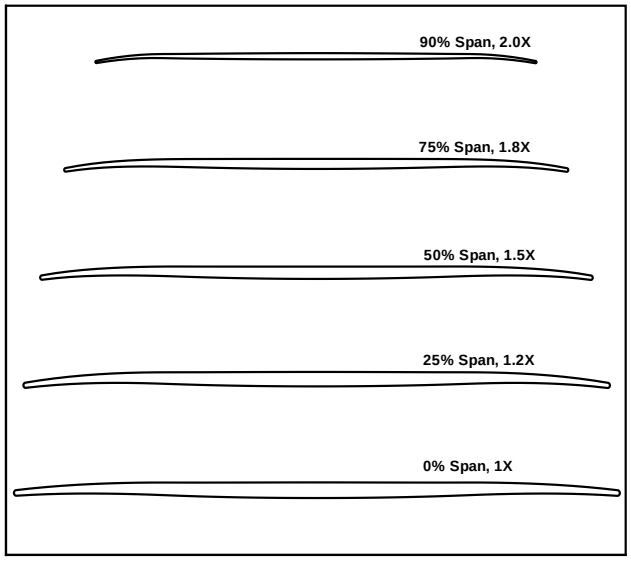

Figure 20: Supersonic airfoil shape at different span of D82-78.8.

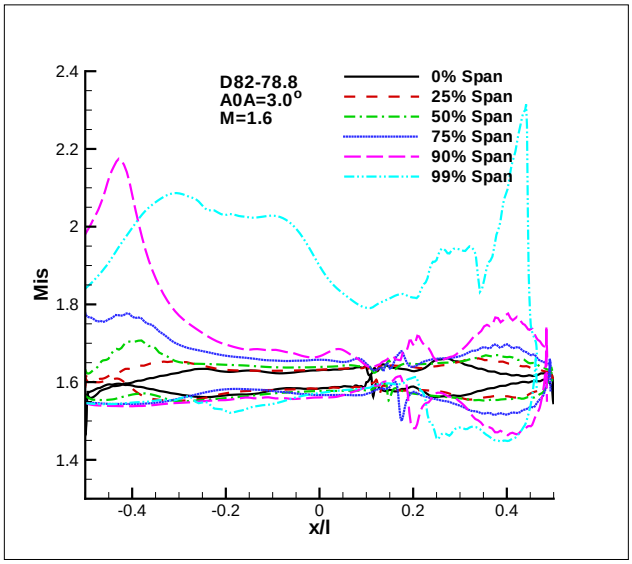

Figure 21: Chordwise isentropic Mach number distributions at different span of D82-78.8.

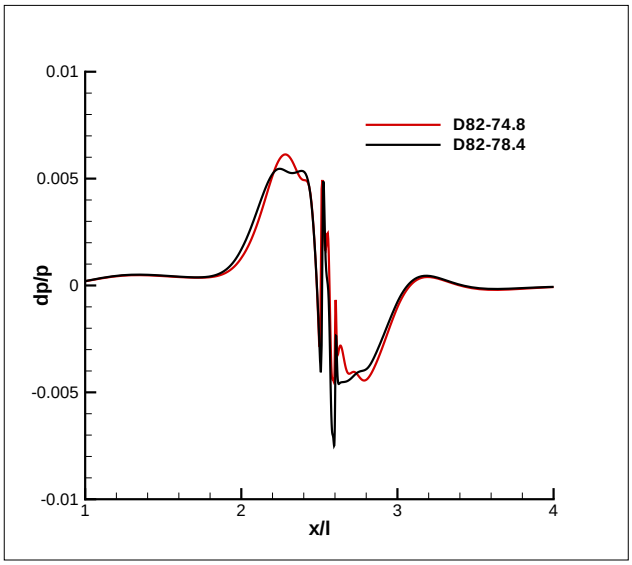

Figure 22: Overpressure two body length below for D82-78.8, $\phi = 0°$.

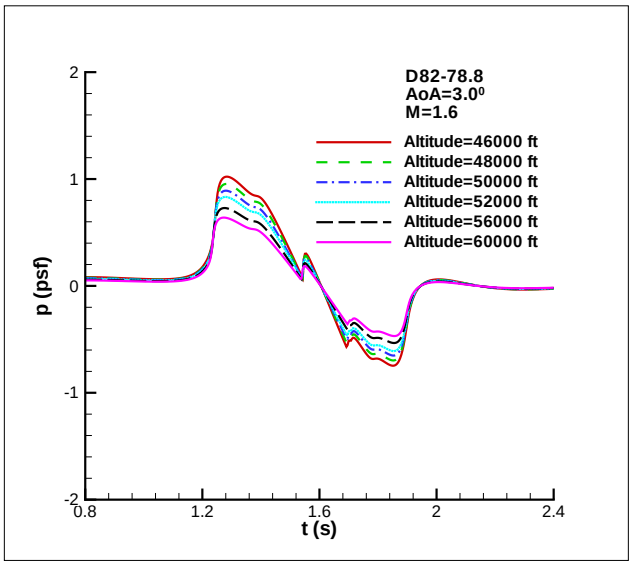

Figure 23: Ground overpressure sonic boom signature of D82-78.8.

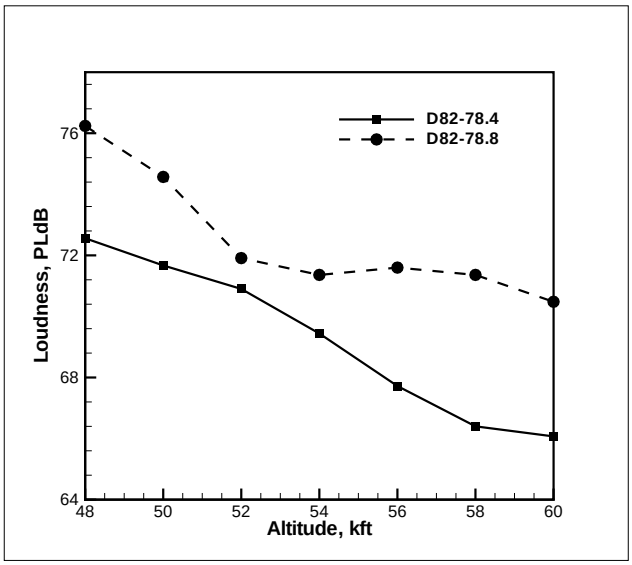

Figure 24: Comparison of ground sonic boom loudness for D82-78.4 and D82-78.8.

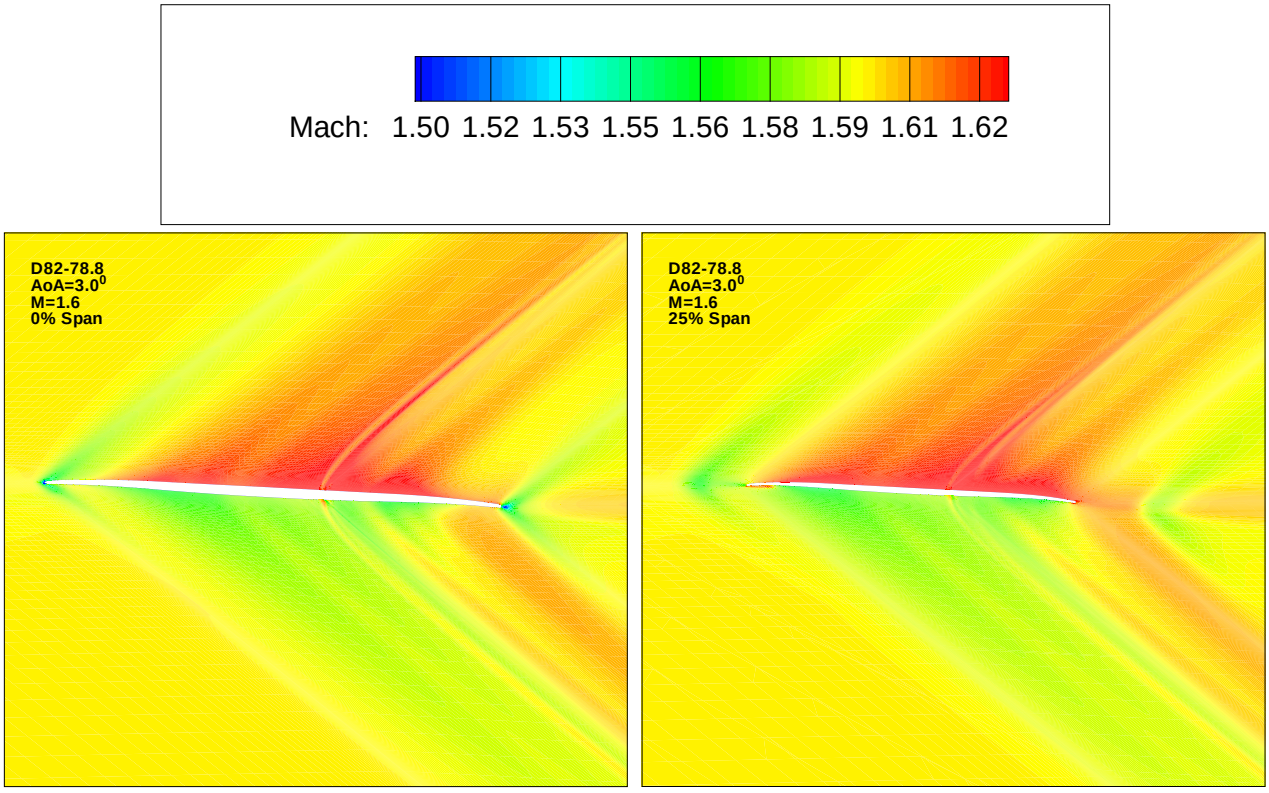

Figure 25: Mach number contours at 0 and 25% span.

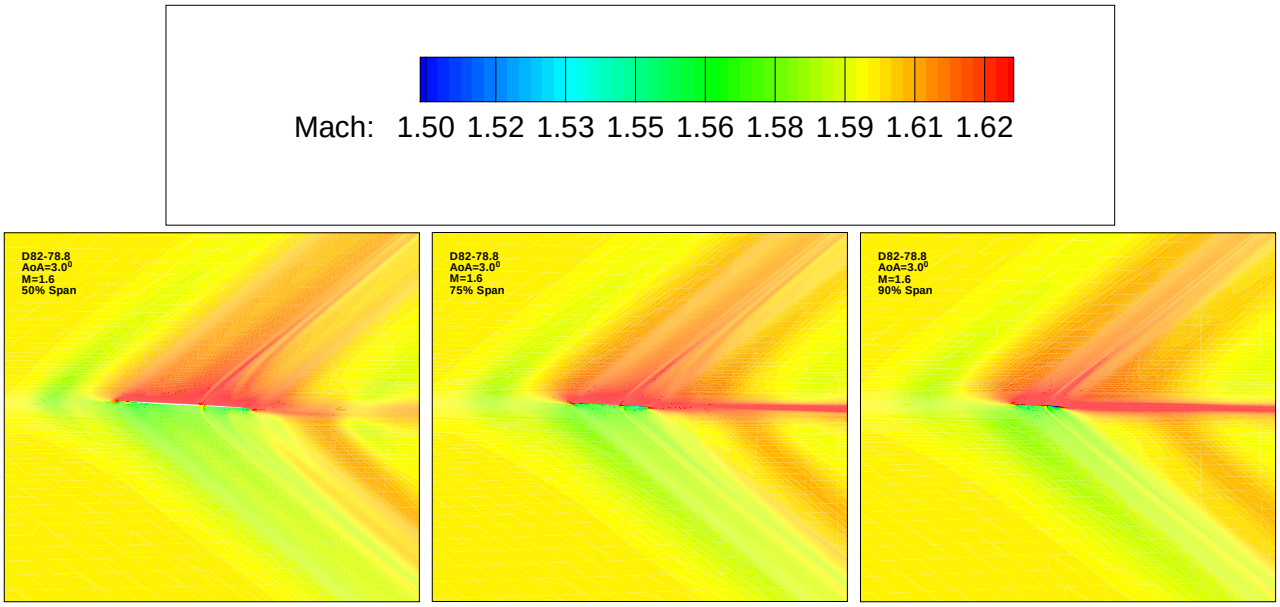

Figure 26: Mach number contours at 50%, 75% and 90% span.

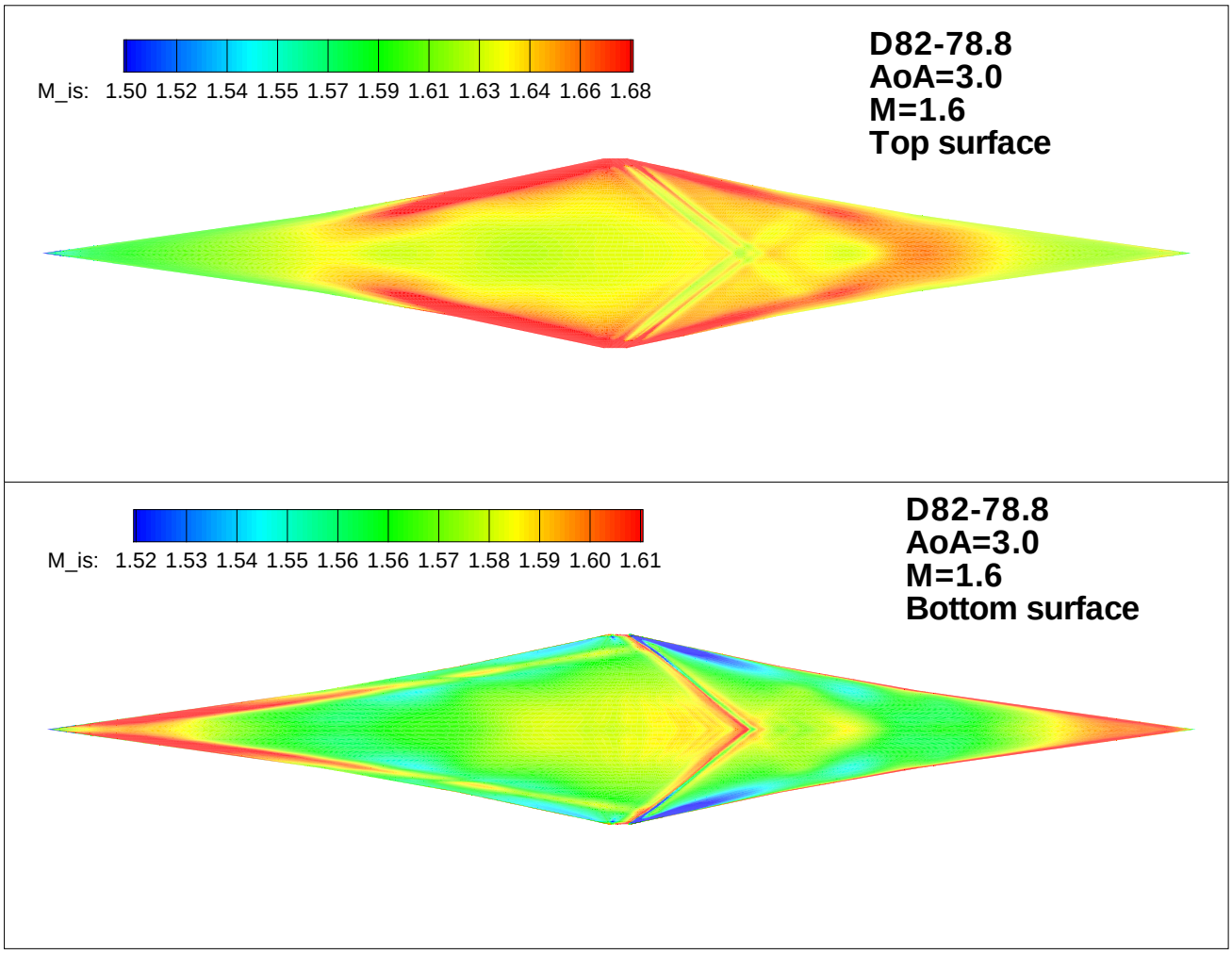

Figure 27: Suction (upper) and pressure (lower) surface isentropic Mach number contours.

References

[1] Hirschberg, M., Hart, D. and Beutner, T., "A Summary Of A Half-Century of Oblique Wing Research." AIAA Paper 2007-150, 2007.

[2] Desktop Aeronautics, Inc., "Oblique Flying Wings: An Introduction and White Paper." http://www.desktopaero.com/obliquewing/library/whitepaper/index.html, 2005.

[3] Campbell, J.P., and Drake, H.M., "Investigation of stability and control characteristics of an airplane model with a skewed wing in the Langley free flight tunnel." NACA TN-1208, May 1947.

[4] Matthews, H. , "Oblique Wing Research Aircraft NASA AD-1." World X-Planes Magazine, No. 2, 2005.

[5] Kroo, I.M., "The Aerodynamic Design of Oblique Wing Aircraft." Proceedings of the AIAA/AHS/ASEE Aircraft Systems Design and Technology Meeting, CP 86-2624, AIAA, Washington D.C., 2005.

[6] Kennelly, R.A., Carmichael, R., Strong, J., and Kroo, I.M., "Transonic Wind Tunnel Test of a 14% Thick Oblique Wing." NASA TM-102230, Aug. 1990.

[7] Kempel, R.W., McNeill, W.E., and Maine, T.A., "Oblique-Wing Research Aircraft Motion Simulation with Decoupling Control Laws." AIAA Paper 88-402, 1988.

[8] Welge, H. R. and Nelson, C. and Bonet, J., "Supersonic Vehicle Systems for the 2020 to 2035 Timeframe." AIAA 2010-4930, 28th AIAA Applied Aerodynamics Conference, Chicago, Illinois, 28 June - 1 July 2010.

[9] Magee, T. E. and Shaw, S. G. and Fugal, S. R., "Experimental Validations of a Low-Boom Aircraft Design." AIAA 2013-0646, 51st AIAA Aerospace Sciences Meeting including the New Horizons Forum and Aerospace Exposition, Grapevine, TX, 07-10 Jan. 2013.

[10] Magee, T. E., Fink, L. E., Fugal, S. P., Adamson, E. E. and Shaw, S. G. , "Boeing N+2 Supersonic Experimental Validation Phase II Program ." 32nd AIAA Applied Aerodynamics Conference, Atlanta, GA, 16-20 June 2014.

[11] Morgenstern, J. M.and Buonanno, M. Chai, S. and Marconi, F. , "Overview of Sonic Boom Reduction Efforts on the Lockheed martin N+2 Supersonic Validations Program." 32nd AIAA Applied Aerodynamics Conference, Atlanta, GA, 16-20 June 2014.

[12] Alonso, J. J. and Colonno, M. R., " Multidisciplimary Optimization with Applications to Sonic-Boom Minimization ," *Annual Review of Fluid Mechanics*, vol. 44, pp. 505–26, 2012.

[13] L. B. Jones, " Lower Bounds for Sonic Bangs ," *Journal of the Royal Aeronautical Society*, vol. 65, 606, pp. 433–436, 1961.

[14] R. Seebass, " Sonic-Boom Theory ," *AIAA Journal of Aircraft*, vol. May-June, pp. 177–184, 1969.

[15] A. George and R. Seebass, " Sonic Boom Minimization including Both Front and Rear Shocks ," *AIAA Journal*, vol. 9, 10, pp. 2091–2093, 1971.

[16] R. Seebass and A. George, " Sonic-Boom Minimization ," *Journal of the Royal Aeronautical Society of America*, vol. 51, 2, pp. 686–694, 1972.

[17] Darden, C. M., "Minimization of Sonic-Boom Parameters in Real and Isothermal Atmospheres." NASA TN D-7842, March 1975.

[18] Darden, C. M., "Sonic-Boom Minimization With Nose-Bluntness Relaxation." NASA TP-1348, January 1979.

[19] Howe, D., Simmons, F., and Freund, D., "Development of the Gulfstream Quiet SpikeTM for Sonic Boom Minimization." AIAA Paper 2008-124, 2008, 7-10, Jan. 2008.

[20] Morgenstern, J. M., "Optimum Signature Shaping for Low Sonic Boom." AIAA 2012-3218, 30th AIAA Applied Aerodynamics Conference, New Orleans, Louisiana, 25 - 28 June 2012.

[21] Whitham, G., " The flow pattern of a supersonic projectile ," *Commun. Pure Appl. Math.*, vol. 5, pp. 301–48, 1952.

[22] M. K. Chan, "Supersonic Aircraft Optimization for Minimizing Drag and Sonic Boom." Ph.D. Thesis, Dept. of Aeronautics and Astronautics, Stanford University, Aug. 2003.

[23] NASA, "NASA Research Announcement ROA-2008 Appendix A.4 Supersonics, Amendment 7, 1. Project Overview." 2008.

[24] Morgenstern, J. M.and Buonanno, M. and Nordstrud, N., "N+2 Low Boom Wind Tunnel Model Design and Validation." AIAA 2012-3217, 30th AIAA Applied Aerodynamics Conference, New Orleans, Louisiana, 25 - 28 June 2012.

[25] Gan, J.-Y. and Lefebvre, A. and Espinal, D. and Zha, G.-C. , "Parametric Trade Study for Supersonic Bi-Directional Flying Wing." AIAA Paper 2014-2106, 32nd AIAA Applied Aerodynamics Conference, Atlanta, GA, 16-20 June 2014.

[26] Zha, G.-C. and Cattafesta, L. and Alvi, F. S. , "Silent and Efficient Supersonic Bi-Directional Flying Wing." Final Report for NASA NIAC Phase I Grant NNX12AR05G8, 9 July, 2013.

[27] Zha, G.-C., " Supersonic Flying Wing with Low Sonic Boom, Low Wave Drag, and High Subsonic Performance (SFW-L^{2}HSP)." Technology Transfer Office UMI-163, University of Miami,FL, Dec. 2008.

[28] Zha, G.-C., " Supersonic Bi-Directional Flying Wing." Provisional patent application No. 61172929, Submitted to USPTO, 27 Apr. 2009.

[29] Zha, G.-C., " Toward Zero Sonic-Boom and High Efficiency Supersonic UAS: A Novel Concept of Supersonic Bi-Directional Flying Wing." US Air Force Academic Outreach UAS Symposium, Grand Forks, ND, Aug. 4-6, 2009.

[30] Staton, R. , " Cargo/Transport Statistical Weight Estimation Equations." Vought Aircraft Report 2-59320/9R-50549, 1969.

[31] Staton, R. , " Statistical Weight Estimation Methods for Fighter/Attack Aircraft." Vought Aircraft Report 2-59320/8R-50475, 1968.

[32] Corke, T. C., *Design of Aircraft.* Prentice Hall, 2003.

[33] Z.-J. Hu, M. Zha, G.-C.and Montgomery, T. Roecken, and J. Orosa, "Transonic Compressor Rotor Design Using Non-monotonic Meanline Angle Distribution." ASME Paper GT2007-27994, 2007.

[34] Gan, J.-Y. and Zha, G.-C. , " Near Field Calculation of Sonic Boom for Benchmark Cases." To be presented in SciTech2015, Orlando, FL, Jan. 2015.

[35] Zha, G.-C., Im, H. and Espinal, D., " Supersonic Bi-Directional Flying Wing, Part I: A novel concept for supersonic flight with high efficiency and low sonic boom ." AIAA Paper 2010-1013, 48th AIAA Aerospace Sciences Meeting, Orlando, FL, Jan. 4-6, 2010.

[36] Berger, C. and Carmona, K. and Im, H.-S. and Espinal, D.and Zha, G.-C., " Supersonic Bi-Directional Flying Wing Configuration with Low Sonic Boom and High Aerodynamic Efficiency." AIAA Paper 2011-3663, 29th AIAA Applied Aerodynamics Conference, Honolulu, Hawaii, 27-30 June 2011.

[37] Shen, Y.-Q. and Zha, G.-C. and Wang, B.-Y., " Improvement of Stability and Accuracy of Implicit WENO Scheme," *AIAA Journal*, vol. 47, No. 2, pp. 331–344, 2009.

[38] Shen, Y.-Q. and Zha, G.-C. , " Improvement of the WENO Scheme Smoothness Estimator," *International Journal for Numerical Methods in Fluids*, vol. DOI:10.1002/fld.2186, 2009.

[39] Shen, Y.-Q. and Zha, G.-C., " A Seventh-Order WENO Scheme and Its Applications." Submitted to SIAM Journal on Scientific Computing, Oct. 2010.

[40] B. Van Leer, "Towards the Ultimate Conservative Difference Scheme, III," *Journal of Computational Physics*, vol. 23, pp. 263–75, 1977.

[41] Y.-Q. Shen and G.-Z. Zha , "Generalized finite compact difference scheme for shock/complex flowfield interaction," *Journal of Computational Physics*, vol. doi:10.1016/j.jcp.2011.01.039, 2011.

[42] Shen, Y.-Q. and Zha, G.-C. and Chen, X.-Y., " High Order Conservative Differencing for Viscous Terms and the Application to Vortex-Induced Vibration Flows," *Journal of Computational Physics*, vol. 228(2), pp. 8283–8300, 2009.

[43] Y.-Q. Shen and G.-C. Zha, "Large Eddy Simulation Using a New Set of Sixth Order Schemes for Compressible Viscous Terms ," *Journal of Computational Physics*, vol. 229, pp. 8296–8312, 2010.

[44] P. Roe, "Approximate Riemann Solvers, Parameter Vectors, and Difference Schemes," *Journal of Computational Physics*, vol. 43, pp. 357–372, 1981.

[45] G.-C. Zha, Y. Shen, and B. Wang, "An improved low diffusion E-CUSP upwind scheme ," *Journal of Computer & Fluids*, vol. 48, pp. 214–220, 2011.

[46] Im, H-S., Chen, X-Y and Zha, G-C., " Detached Eddy Simulation of Rotating Stall Inception for a Full Annulus Transonic Rotor ," *AIAA Journal of Propulsion and Power*, vol. 28, No. 4, pp. 782–798, 2012.

[47] Im, H-S., Chen, X-Y., and Zha, G-C., "Prediction of a Supersonic Wing Flutter Boundary Using a High Fidelity Detached Eddy Simulation." AIAA Paper 2012-0039, 50th AIAA Aerospace Sciences Meeting, Tennessee,TN, submitted to AIAA Journal, 9-12 January 2012.

[48] Wang, B. Y and Zha, G.-C., "Detached-Eddy Simulation of Transonic Limit Cycle Oscillations Using High Order Schemes," *Journal of Computer & Fluids*, vol. 52, pp. 58–68, 2011.

[49] Wang, B. Y and Zha, G.-C., "Detached-Eddy Simulation of a Co-Flow Jet Airfoil at High Angle of Attack," *AIAA Journal of Aircraft*, vol. 48, 5, pp. 1495–1502, 2011.

[50] Im, H. and Zha, G., "Delayed Detached Eddy Simulation of the Aerodynamic Stall Flows Over the NACA0012 Airfoil." AIAA Paper 2011-1297, 49th AIAA Aerospace Sciences Meeting including, Orlando, Florida, 4 - 7 Jan 2011.

[51] Im, H-S. Chen, X.-Y. and Zha, G-C., "Simulation of 3D Multistage Axial Compressor Using a Fully Conservative Sliding Boundary Condition." ASME-IMECE 2011-62049, Proceedings of the ASME 2011 International Mechanical Engineering Congress & Exposition IMECE2011, Denver, Colorado, USA, Nov. 11-17, 2011.

[52] Im, H-S., Chen, X-Y and Zha, G-C., " Detached Eddy Simulation of Transonic Rotor Flutter Using a Fully Coupled Fluid-Structural Interaction ." ASME Paper GT2011-45437, ASME TURBO EXPO 2011, June 6-10, Vancouver, Canada, June 6-10, 2011.

[53] Im, H.-S. and Zha, G.-C. and Dano, B. P. E., "Large Eddy Simulation of Coflow Jet Airfoil at High Angle of Attack," *Journal of Fluid Engineering*, vol. 136(2), p. 021101, 2014.

[54] Wang, B. Y and Zha, G.-C., "High Fidelity Simulation of Nonlinear Fluid-Structural Interaction with Transonic Airfoil Limit Cycle Oscillations," *Journal of Fluids and Structures*, vol. doi:10.1016/j.jfluidstructs.2010.02.003, 2010.

[55] Wang, B.-Y. and Haddoukessouni, B. and Levy, J. and Zha, G.-C., "Numerical Investigations of Injection Slot Size Effect on the Performance of Co-Flow Jet Airfoil ," *AIAA Journal of Aircraft*, vol. 45, pp. 2084–2091, 2008.

[56] X.-Y. Chen, G.-C. Zha, and M.-T. Yang, "Numerical Simulation of 3-D Wing Flutter with Fully Coupled Fluid-Structural Interaction," *Journal of Computers & Fluids*, vol. 36, No. 5, pp. 856–867, 2007.

[57] X.-Y. Chen and G.-C. Zha, "Fully Coupled Fluid-Structural Interactions Using an Efficient High Resolution Upwind Scheme," *Journal of Fluids and Structures*, vol. 20, pp. 1105–1125, 2005.

[58] Z.-J. Hu and G.-C. Zha, "Calculations of 3D Compressible Using an Efficient Low Diffusion Upwind Scheme," *International Journal for Numerical Methods in Fluids*, vol. 47, pp. 253–269, 2004.

[59] Im, H-S. and Zha, G-C., "Effects of Rotor Tip Clearance on Tip Clearance Flow Potentially Leading to NSV in an Axial Compressor." ASME Paper GT2012-68148, IGTI Turbo Expo 2012, Copenhagen, Denmark, June 11-15, 2012.

[60] Im, H-S. and Zha, G-C., "Simulation of Non-synchronous Blade Vibration of an Axial Compressor Using a Fully Coupled Fluid-Structural Interaction." ASME Paper GT2012-68150, IGTI Turbo Expo 2012, Copenhagen, Denmark, June 11-15, 2012.

[61] B.-Y. Wang and G.-C. Zha, "A General Sub-Domain Boundary Mapping Procedure For Structured Grid CFD Parallel Computation," *AIAA Journal of Aerospace Computing, Information, and Communication*, vol. 5, No.11, pp. 2084–2091, 2008.

[62] Winter, K. G. and Smith, K. G., "Measurements of Skin Friction on a Cambered Delta Wing at Supersonic Speeds." R. & M. No. 3501, AERONAUTICAL RESEARCH COUNC1L, LONDON, HER MAJESTY'S STATIONERY OFFICE, August 1965.

[63] Park, M. A., "Low Boom Configuration Analysis with FUN3D Adjoint Simulation Framework." AIAA 2011-3337, 29th AIAA Applied Aerodynamics Conference, Honolulu, Hawaii, June 2011.

[64] Seebass, R., "Supersonic Aerodynamics: Lift and Drag ." Paper presented at the RTO AVT Course on *Fluid Dynamics Research on Supersonic Aircraft*, RTO EN-4, Rhode-Saint-Gendse, Belgium,, 25-29 May 1998.

[65] Rallabhandi, S. K., "Advanced Sonic Boom Prediction Using Augmented Burger's Equation." 49th AIAA Aerospace Sciences Meeting including the New Horizons Forum and Aerospace Exposition, Orlando, Florida, Jan. 4-7, 2011.